Land Subsidence Estimation With Tide Gauge and Satellite Radar Altimetry Measurements Along the Texas Gulf Coast, USA

Xiaojun Qiao, Tianxing Chu, Philippe Tissot, Jason Louis, and Ibraheem Ali

***Abstract*— A double-difference (DD) method was used to estimate vertical land motion (VLM) at 26 tide gauge (TG) sites with record lengths of at least ten years across the Texas Gulf Coast, USA, between 1993 and 2020. In the method, the first difference was conducted by coupling nearby correlated TG stations to remove sea-level variability for both TG and satellite radar altimetry (SRA) data. Upon completion of the first difference, a second difference was performed by subtracting between TG and SRA data. The results obtained from the DD method were compared against that of: 1) a single-difference (SD) method through subtraction between measurements from TG and SRA and 2) a global navigation satellite system (GNSS) precise point positioning (PPP) method. The results showed that the DD method improved the performance of VLM estimation with an uncertainty below 1.0 mm/yr at most TG stations. Meanwhile, the estimated VLM trends acquired from the DD method correlated better to that of the ground-truth GNSS PPP solutions than the SD method. The DD method possesses great potential to discover VLM knowledge, particularly along coastal regions where other techniques such as GNSS and interferometric synthetic aperture radar (InSAR) are of impaired estimation capability.**

***Index Terms*— Coastal subsidence, double-difference (DD), radar altimetry, tide gauge (TG).**

I. Introduction

A COASTLINE defines the boundary between land and sea water. Around 10% of the world population lives in coastal zones with elevation below 10 m [1]. Nowadays, some coastal communities are becoming more vulnerable than ever due to continuous relative water–land movement such as land subsidence. Land subsidence spells the loss of freeboard, which is the elevation of the land above mean sea level [2]. It can lead to increased flood risks and cause significant impacts on ecosystem resilience, near-shore infrastructures, daily lives of coastal residents, etc. For coastal areas that suffer from land subsidence, it is of growing significance to accurately model and estimate the patterns of subsidence and provide such knowledge to pertinent stakeholders in a timely fashion to assist the decision-making process.

The global navigation satellite system (GNSS) and interferometric synthetic aperture radar (InSAR) are two leading direct methods for monitoring land subsidence in academia. Continuously operating GNSS network (cGNSS) can provide accurate subsidence observations at selected stations. However, the number of stations that were installed near a coastline with relatively long observation history (e.g., 15 years or longer) tends to be limited [3]. Due to the highly variable nature of land subsidence [4], it is challenging to recover a subsidence map with a sparse cGNSS coverage along the coast. On the other hand, multitemporal InSAR is capable of effectively mapping large-scale land deformation. However, it likely requires high professionalism and high-performance computing resources in image processing. In addition, applications that require seamless InSAR analysis over a long period of time may need imagery across various synthetic aperture radar (SAR) platforms [5], which can further exacerbate the processing complexity.

As opposed to the above-referenced methods, coastal subsidence can also be indirectly estimated with sea-level measurements. Tide gauges (TGs) are attached to the land and measure sea-level changes relative to land-fixed benchmarks, referred to as relative sea-level rise (RSLR). To be specific, RLSR aggregates the effects of subsidence from coastal land and absolute sea-level rise (ASLR) from the ocean. ALSR reflects sea surface height changes relative to a well-defined geocentric reference frame, mainly resulting from the globally continuous glacier mass loss and ocean thermal expansion [6]. Satellite radar altimetry (SRA) technique makes it possible to track the changes in sea surface height since 1990s, which can be used to estimate the spatial and temporal variabilities of ASLR for nearly 30 years. Conceptually, time series difference between ASLR and RSLR measurements reflects the outcomes of vertical land motion (VLM).

Prior studies have investigated the feasibility of estimating VLM via the single difference (SD) between SRA and TG observations [7]. However, large noise contained in the time series of the SD results posed a challenge in confidently estimating the VLM estimation trend [8]. To decrease the residuals of sea-level variations, a network adjustment strategy was developed based on double-differenced measurements

Manuscript received 28 April 2022; revised 21 June 2022; accepted 23 July 2022. Date of publication 26 July 2022; date of current version 8 August 2022. This work was supported by the U.S. Department of Commerce-National Oceanic and Atmospheric Administration (NOAA) through the University of Southern Mississippi (USM) under Agreement NA13NOS4000166. *(Corresponding author: Tianxing Chu.)*

Xiaojun Qiao and Tianxing Chu are with the Department of Computing Sciences and the Conrad Blucher Institute for Surveying and Science, Texas A&M University-Corpus Christi, Corpus Christi, TX 78412 USA (e-mail: xqiao@islander.tamucc.edu; tianxing.chu@tamucc.edu).

Philippe Tissot is with the Department of Physical and Environmental Sciences and the Conrad Blucher Institute for Surveying and Science, Texas A&M University-Corpus Christi, Corpus Christi, TX 78412 USA (e-mail: philippe.tissot@tamucc.edu).

Jason Louis and Ibraheem Ali are with the Conrad Blucher Institute for Surveying and Science, Texas A&M University-Corpus Christi, Corpus Christi, TX 78412 USA (e-mail: jason.louis@tamucc.edu; ibraheem.ali@tamucc.edu).

Digital Object Identifier 10.1109/LGRS.2022.3194108

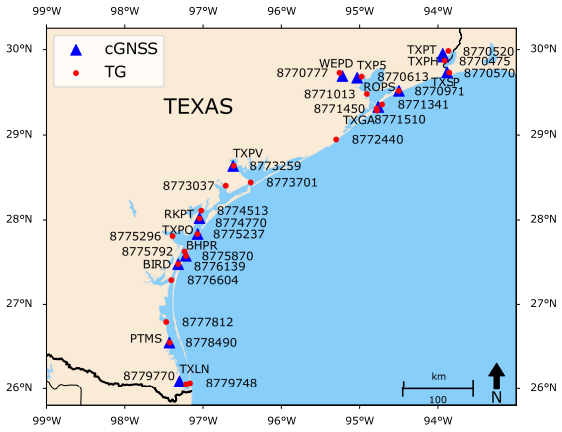

Fig. 1. Distribution of TGs (marked with numerical identities) and cGNSS stations for validation (marked with four-letter identities) along the Texas Gulf Coast, USA.

over predefined coastal regions [9]–[11]. Specifically, the first difference is between TG and SRA observations independently for each station, and a second difference was conducted between paired TG stations upon completion of the first difference. However, only TG stations with at least 40 years of observations were used to have consistent estimated trends with negligible influence from interdecadal sea-level fluctuations. It should be noted that there is approximately only one-third of global TG stations with observation records of over 40 years [12]. The VLM estimated using new TG stations that were installed within the recent decade may be subject to adverse influence of low-frequency (i.e., interdecadal) sea-level variations.

To mitigate this impact for reliable VLM knowledge discovery, this study uses a double-difference (DD) method to document reliable VLM processes. Different from prior studies that developed the DD method with network adjustment for VLM estimation [9], [10], this investigation aims at leveraging SRA data along with measurements from a cluster of correlated TG stations, including those with relatively short observation period. Specifically, this study examines VLM at 26 TG stations with record length of at least ten years between 1993 and 2020 along the Texas Gulf Coast, one of the subsiding hotspots in the United States.

II. Data

Six-minute or hourly water-level data above the mean lower low water (MLLW) datum were downloaded for 26 TG stations along the entire Texas Gulf Coast, USA (Fig. 1), from the Center for Operational Oceanographic Products and Services (CO-OPS) at National Oceanic and Atmospheric Administration (NOAA). Each TG station had a record length of at least ten years ranging between 1993 and 2020. TG data of each station were averaged to daily water-level measurements. It is worth noting that two TGs (named as 8772440 and 8772447 by NOAA) near Freeport, TX, were synthesized as a single station considering their short distance (around 0.8 km) and each recording nearly one half of the period from 1993 to 2020. To normalize water-level measurements across all TG stations, the mean value of the entire time series was calculated and subtracted from daily water-level observations for each station.

The ASLR data, estimated with the level-4 SRA product, between January 1993 and March 2020 over the Gulf of Mexico (GOM) region, were produced by the Copernicus Marine Environment Monitoring Service (CMEMS) [13]. Daily sea-level anomalies regarding a 20-year (i.e., from 1993 to 2012) mean were provided for each 0.25° × 0.25° grid cell in the level-4 product, which was interpolated based on the level-3 product. Dynamic atmospheric correction (DAC) was included in the level-3 product to account for water level responding to atmospheric wind and pressure forcing. DAC was compensated before differencing sea-level measurements between TG and SRA and was acquired from the Archiving, Validation, and Interpretation of Satellite Oceanographic (AVISO) [14]. Four DAC values per day since 1992 were averaged to daily mean within each 0.25° × 0.25° grid cell.

To validate the performance of the VLM estimation methods to be used in this study, positioning results from 14 cGNSS stations along the Texas coastline were leveraged (Fig. 1). Specifically, geodetic-grade positioning results from ten of these cGNSS stations (i.e., TXPT, TXPH, TXSP, TXP5, WEPD, TXGA, TXPV, TXPO, TXLN, and TXRP) were directly accessed and used for validation [15]. In addition, raw observations from five more stations (i.e., ROPS, RKPT, BHPR, BIRD, and PTMS) installed and independently operated by Conrad Blucher Institute for Surveying and Science (CBI) at Texas A&M University-Corpus Christi (TAMU-CC) were accessed and postprocessed via precise point positioning (PPP) technique.

It should be noted that the TXRP station, located within the city limits of Rockport, TX, was damaged in August 2017 due to Hurricane Harvey, resulting in continuous data outages afterward. On the other hand, the RKPT station, 0.5 km away from TXRP, started to collect data after April 2017. RKPT and TXRP shared a few months of observation overlap in 2017, and their GNSS positioning results were, therefore, merged for comparison against VLM estimated with the corresponding SRA grid cell and TG station (named as 8774770 by NOAA) at Rockport, TX. The availability of all GNSS data used in this study was truncated until the end of 2020. Fig. 2 illustrates data availability and overlaps between TGs and cGNSS stations that are in closest proximity.

III. Method

The rates of RSLR change $\dot{R}$ and ASLR change $\dot{A}$ satisfy [9]

$$\dot{U} = \dot{A} - \dot{R} \tag{1}$$

where $\dot{U}$ is the VLM rate, and $\cdot$ superscript denotes the temporal trend. In this study, the VLM time series was estimated with a DD method as shown in (2), where the first difference served to mitigate sea-level variability in ASLR and RSLR, respectively, and the second difference was to calculate the offset between ASLR and RSLR

$$U(t) = \left[A(t) - V^A(t)\right] - \left[R(t) - D(t) - V^R(t)\right]. \tag{2}$$

Fig. 2. Observation availability and overlaps between TGs (green) and cGNSS stations (orange or magenta) that are in closest proximity.

In (2), t depicts time, $A(t)$ and $R(t)$ are ASLR and RSLR time series data, respectively, $D(t)$ represents the daily DAC values to compensate the correction included in the ASLR product, and $V^A(t)$ and $V^R(t)$ denote the temporal variability of ASLR and RSLR at the TG station under investigation, respectively. $V^A(t)$ and $V^R(t)$ are calculated in (3)

$$\begin{cases} V^A(t) = \dfrac{1}{m}\displaystyle\sum_{i=1}^{m} \tilde{A}_i(t), \quad V^R(t) = \dfrac{1}{m}\displaystyle\sum_{i=1}^{m} \tilde{R}_i(t) \quad (m > 0) \\ V^A(t) = 0, \qquad\qquad\qquad V^R(t) = 0 \quad (m = 0) \end{cases} \tag{3}$$

where m represents the number of selected TGs, $Q = \{Q_1, Q_2, \ldots, Q_m\}$, from a set of eight candidate stations, C, that have stored observation records for over 25 years as evidenced in Fig. 2. However, compared with nearby TG stations, the one (named as 8771013 by NOAA) at San Leon, TX, exhibited obvious nonlinear land motion processes other than interannual to decadal fluctuations [16] and was, therefore, excluded from the set C. In this study, $m \leq 7$ was concluded. $\tilde{R}_i(t)$ is the detrended RSLR time series for each selected TG station, $Q_i \in Q \subseteq C$, as defined in (4). $\tilde{A}_i(t)$ is the detrended ASLR time series of the SRA grid cell, $A_i(t)$, that is in closest proximity to Q_i, where $i \in \{1, 2, \ldots, m\}$

$$\begin{cases} \tilde{A}_i(t) = A_i(t) - f_i(t) \\ \tilde{R}_i(t) = R_i(t) - g_i(t). \end{cases} \tag{4}$$

In (4), $f_i(t)$ and $g_i(t)$ are linear fit functions for ASLR and RSLR, respectively. Algorithm 1 summarizes how to select the set $Q \subseteq C$ to calculate $V^A(t)$ and $V^R(t)$ in (3).

Algorithm 1 Selection of TG Candidates

$TG\_c \leftarrow$ the TG station under investigation
$C \leftarrow$ the set of all candidate TG stations
$p \leftarrow$ the number of elements in the set C
$Q \leftarrow \{\}$ //The set of selected TG stations
$m \leftarrow 0$ //Number of selected candidate TG stations
$max \leftarrow -1$ //Maximum correlation coefficient
$S \leftarrow \{\}$ //Candidate TG station in C with max
for $k \leftarrow 1$ **to** p **do**
  if $TG\_c \neq C_k$ **then**
    $r_k \leftarrow \text{corr}(TG\_c, C_k)$ // correlation coefficient
    if $r_k \geq 0.9$ **then**
      $Q \leftarrow Q \cup \{C_k\}$
      $m \leftarrow m + 1$
    end
    if $r_k > max$ **then**
      $max \leftarrow r_k$
      $S \leftarrow \{C_k\}$
    end
  end
end
if $m == 0$ **then**
  if $max > 0.8$ **then**
    $Q \leftarrow S$
    $m \leftarrow 1$
  end
end
Result: Q, m

Note the correlation coefficient, r_k, was calculated using daily RSLR time series, after DAC correction, between the current TG station, TG_c, and a candidate station, $C_k \in C$. The current TG station was not considered as a valid candidate, i.e., $TG\_c \notin Q \subseteq C$, for calculating $V^A(t)$ and $V^R(t)$. The optimal thresholds in Algorithm 1 were deliberately selected for successful execution of the DD model for most TG stations in the study while balancing the needs of not degrading the VLM trend estimate using observations from some TG stations with record length merely over ten years [9], [10], [12]. These empirical thresholds may be subject to change depending on a combination of factors such as data length and duration, study location, water-level fluctuations and so forth. For comparison purpose against the DD method, the SD solution for VLM estimation between ASLR and RSLR, as shown in (5), was also used

$$U(t) = A(t) - \big[R(t) - D(t)\big]. \tag{5}$$

The raw data obtained from the cGNSS stations independently operated by CBI within TAMU-CC were post-processed through Jet Propulsion Laboratory (JPL)'s GipsyX software to achieve mm-level positioning ground truth with 24-h GNSS data [17]. Various types of correction models were incorporated in PPP processing, including the second-order ionospheric correction through IONosphere EXchange (IONEX) map and the international reference ionospheric (IRI) model, tropospheric correction through the global pressure and temperature (GPT2) model, ocean-tide loading with the global ocean tide (GOT-4.8) model, etc. The

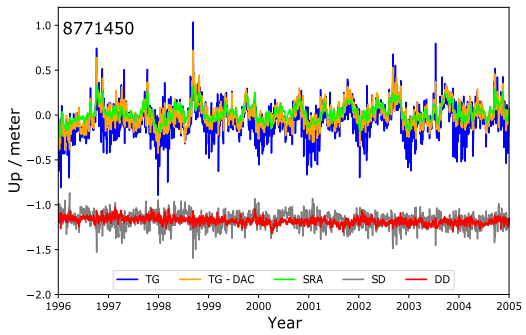

Fig. 3. Daily water-level variations and VLM estimated with the SD and DD methods.

vertical components of the GNSS positioning results were used for validation against that obtained from the DD method.

Hector, a software package capable of analyzing linear regression with temporal correlated noise, was then used to model the VLM trend in time series estimated with the sea-level DD and GNSS methods, respectively. Hector is robust to offsets, outliers, and seasonal signals contained in time series [18], and different noise models and their combinations were examined.

IV. Results

Fig. 3 presents daily water-level variations in ten-year time series for the TG station, named as 8771450 by NOAA, located in Galveston, TX. It is apparent that DAC helped greatly mitigate high-frequency variations, and the time series SRA data agreed well with the TG measurements regarding seasonal changes. While the time series VLM values achieved by the SD and DD methods were comparable, the uncertainty estimated by DD clearly outperformed that of the SD (Fig. 3). To display all curves clearly, an arbitrary vertical offset was applied to both the DD and SD curves, shifting from the sea-level time series. Note that this did not change the nature of the focus in the study for VLM rate and uncertainty estimation.

At each TG station, daily VLM time series were first calculated in DD via (2) and SD via (5). In trend estimation, daily VLM time series of both the SD and DD methods were averaged to monthly mean and were then loaded into Hector. The VLM trend and uncertainty in time series were determined by adopting the optimal noise model in Hector at all 26 TG stations (Fig. 4). The dot in each line depicts the VLM trend within the uncertainty range defined with lower and upper standard deviation bounds. Trend significance of the DD results at each TG station was examined using the Mann–Kendall test (Fig. 4).

It is observed that at most TG stations, the DD method is effective for decreasing the VLM trend uncertainty. However, DD was not applied in two TG stations (i.e., 8770971 and 8777812) due to no correlation with the candidate TGs being greater than 0.8 as introduced in Algorithm 1. Therefore, at these two TGs, the results from the DD and SD methods coincide. Furthermore, the VLM uncertainty estimates at TGs 87746604 and 8779770 remained relatively large. This is because correlated stations are distant (i.e., at least 130 km), amplifying temporal variability between these two TG stations and their corresponding correlated stations [19].

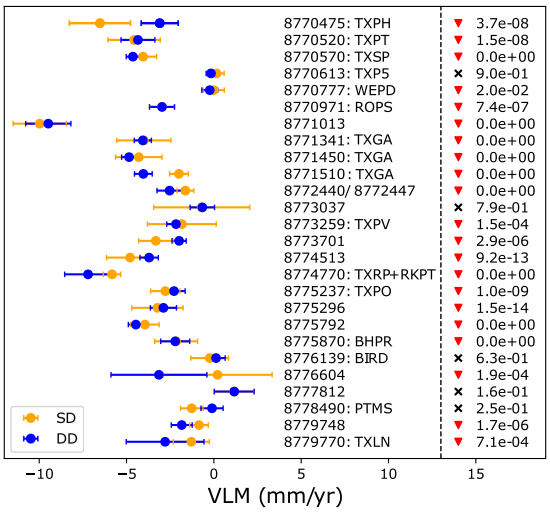

Fig. 4. Left to the vertical dashed line: VLM trend and uncertainty estimated for TGs along the Texas Gulf Coast using the DD and SD methods. Right to the vertical dashed line: results of Mann–Kendall trend test (p-value < 0.05) in the DD method. TGs marked with red triangles are significantly subsided stations. A black cross mark indicates no significant trend. The p-value associated with every TG station is shown to the rightmost of the figure in scientific notation.

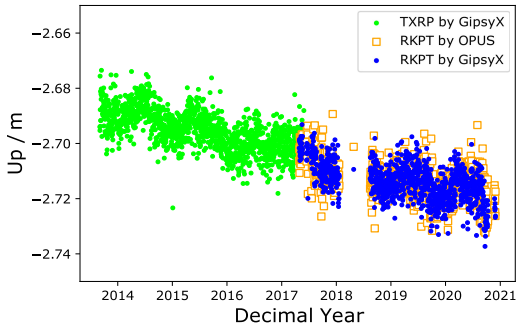

Fig. 5. Time series of daily positions for cGNSS stations near Rockport in the up-direction.

To evaluate the performance of GNSS PPP technique using GipsyX, the up-direction time series was compared against that of NOAA's Online Positioning User Service (OPUS) interface, where high-accuracy coordinates were computed using a localized NOAA continuously operating reference stations (CORS) network [20]. As an example, an accuracy achieved using GipsyX was comparable to that with OPUS at RKPT station (Fig. 5). Consistent results were also documented between TXRP and RKPT, which justified combining results of these two cGNSS stations as explained in Section II. For each cGNSS station, daily time series data were used in Hector for trend estimation.

As indicated in Fig. 4, a total of 16 TG sites were found in close proximity to nearby cGNSS stations regarding the VLM trend comparison. In general, compared with the cGNSS estimate, the DD method yielded a better agreement ($R^2 = 0.58$) than the SD method ($R^2 = 0.46$), where R^2 represents coefficient of determination of the linear regression and the 1:1 dashed line illustrates the most ideal estimation–observation relationship (Fig. 6). Some points are relatively deviated from the 1:1 line, and this is likely because: 1) the length of some TG records was much longer than that of their corresponding nearby cGNSS stations, leading to biased

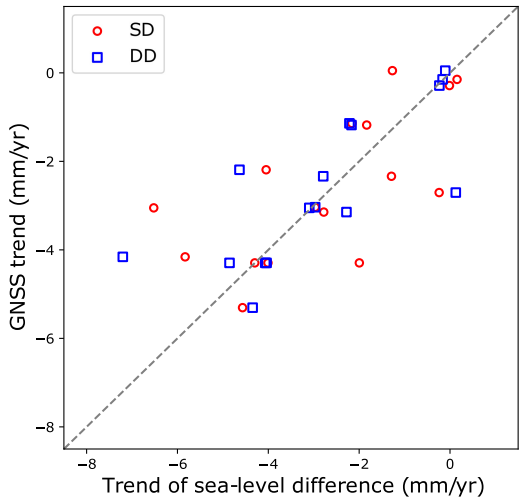

Fig. 6. Scatterplot of VLM trend estimated between cGNSS versus SD and DD methods.

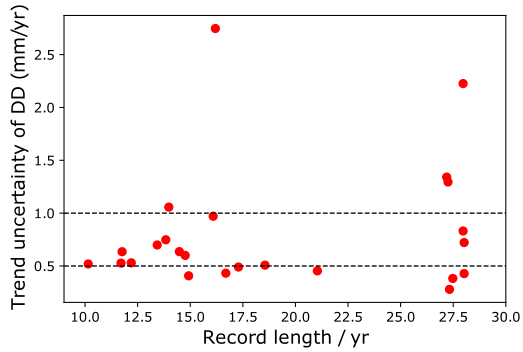

Fig. 7. Trend uncertainty of the DD method at each TG station characterized with the length of data records.

trend estimation; 2) linear VLM trend was hypothesized while nonlinear sea-level difference data were observed for some stations; and 3) subsidence patterns may vary spatially between the TG and the corresponding nearby cGNSS stations.

Fig. 7 depicts the trend uncertainty of the DD method at each TG station characterized with the length of data records. The results of two TG stations (i.e., 8770971 and 8777812) are not present because the DD method did not apply to them as explained in Section IV. It is visible that nearly 30% and 80% of TG stations yielded a trend uncertainty estimate of lower than 0.5 and 1.0 mm/yr using the DD method, respectively. However, there are two TG stations that exceeded 2.0 mm/yr uncertainty due to the reason explained earlier.

V. Conclusion

In this study, a DD method was used to estimate VLM trend across the Texas coastline at 26 TG stations with record length of over ten years along with SRA datasets. VLM trend results at 16 TG stations were compared against that obtained from their corresponding near located cGNSS stations. It was documented that the DD method yielded a better correlation with GNSS than the SD method (i.e., $R^2 = 0.58$ and 0.46, respectively). Relative to the SD method, the uncertainty of the trend estimation acquired from the DD method was generally improved, achieving a level of below 1.0 mm/yr at most TGs. The DD method possesses great potential to complement cGNSS and InSAR techniques in providing VLM knowledge, especially along coastlines where TG measurements are available. To mitigate the impact of the spatial and temporal variability on land subsidence, future efforts should focus on long-term and high-resolution estimation by coupling multiple sources of geospatial data. More exploration is also needed in investigating natural and anthropogenic factors that lead to land subsidence.

References

[1] G. Mcgranahan, D. Balk, and B. Anderson, "The rising tide: Assessing the risks of climate change and human settlements in low elevation coastal zones," *Environ. Urbanization*, vol. 19, pp. 17–37, Apr. 2007.

[2] P. G. Eriksson, "Sea level changes and the continental freeboard concept: General principles and application to the precambrian," *Precambrian Res.*, vol. 97, nos. 3–4, pp. 143–154, Sep. 1999.

[3] J. Yu and G. Wang, "Introduction to the GNSS geodetic infrastructure in the Gulf of Mexico region," *Surv. Rev.*, vol. 49, no. 352, pp. 51–65, Jan. 2017.

[4] P. Castellazzi *et al.*, "Land subsidence in major cities of central Mexico: Interpreting InSAR-derived land subsidence mapping with hydrogeological data," *Int. J. Appl. Earth Observ. Geoinf.*, vol. 47, pp. 102–111, May 2016.

[5] F. Qu *et al.*, "Mapping ground deformation over Houston–Galveston, Texas using multi-temporal InSAR," *Remote Sens. Environ.*, vol. 169, pp. 290–306, Nov. 2015.

[6] T. Frederikse *et al.*, "The causes of sea-level rise since 1900," *Nature*, vol. 584, no. 7821, pp. 393–397, Aug. 2020.

[7] A. Cazenave, K. Dominh, F. Ponchaut, L. Soudarin, J. F. Cretaux, and C. Le Provost, "Sea level changes from Topex-Poseidon altimetry and tide gauges, and vertical crustal motions from DORIS," *Geophys. Res. Lett.*, vol. 26, no. 14, pp. 2077–2080, Jul. 1999.

[8] X. Qiao, T. Chu, P. Tissot, and J. Louis, "Land subsidence with tide gauge, radar altimetry and GNSS: A case study at subsiding coast in Texas," in *Proc. 34th Int. Tech. Meeting Satell. Division Inst. Navigat. (ION GNSS)*, Oct. 2021, pp. 3956–3962.

[9] C. Kuo, C. Shum, A. Braun, and J. Mitrovica, "Vertical crustal motion determined by satellite altimetry and tide gauge data in fennoscandia," *Geophys. Res. Lett.*, vol. 31, no. 1, pp. 1–4, 2004.

[10] C. Letetrel, M. Karpytchev, M.-N. Bouin, M. Marcos, A. Santamarìa-Gómez, and G. Wöppelmann, "Estimation of vertical land movement rates along the coasts of the Gulf of Mexico over the past decades," *Continental Shelf Res.*, vol. 111, pp. 42–51, Dec. 2015.

[11] F. De Biasio, G. Baldin, and S. Vignudelli, "Revisiting vertical land motion and sea level trends in the northeastern Adriatic sea using satellite altimetry and tide gauge data," *J. Mar. Sci. Eng.*, vol. 8, no. 11, p. 949, Nov. 2020.

[12] G. Wöppelmann and M. Marcos, "Vertical land motion as a key to understanding sea level change and variability," *Rev. Geophys.*, vol. 54, no. 1, pp. 64–92, Mar. 2016.

[13] E. U. Copernicus Marine Service Information. *Global Ocean Gridded L4 Sea Surface Heights and Derived Variables Reprocessed (1993-Ongoing)*. Accessed: Mar. 9, 2022. [Online]. Available: https://doi.org/10.48670/moi-00148

[14] LEGOS/CNRS/CLS. (1992). *Dynamic Atmospheric Correction*. [Online]. Available: https://www.aviso.altimetry.fr/en/data/products/auxiliary-products/dynamic-atmospheric-correction.html

[15] G. Blewitt, W. Hammond, and C. Kreemer, "Harnessing the GPS data explosion for interdisciplinary science," *Eos*, vol. 99, p. 485, Sep. 2018.

[16] B. Douglas, M. S. Kearney, and S. P. Leatherman, *Sea Level Rise: History and Consequences*. Amsterdam, The Netherlands: Elsevier, 2000.

[17] W. Bertiger *et al.*, "GipsyX/RTGx, a new tool set for space geodetic operations and research," *Adv. Space Res.*, vol. 66, no. 3, pp. 469–489, Aug. 2020.

[18] M. S. Bos, R. M. S. Fernandes, S. D. P. Williams, and L. Bastos, "Fast error analysis of continuous GNSS observations with missing data," *J. Geodesy*, vol. 87, no. 4, pp. 351–360, Apr. 2013.

[19] B. C. Douglas, "Global sea level rise," *J. Geophys. Res., Oceans*, vol. 96, no. C4, pp. 6981–6992, 1991.

[20] D. T. Gillins, D. Kerr, and B. Weaver, "Evaluation of the online positioning user service for processing static GPS surveys: OPUS-projects, OPUS-S, OPUS-net, and OPUS-RS," *J. Surveying Eng.*, vol. 145, no. 3, Aug. 2019, Art. no. 05019002.